Vol 16 No 11, November 2007
1009-1963/2007/16(11)/3475-08

Chinese Physics

© 2007 Chin. Phys. Soc.
and IOP Publishing Ltd

Investigation of vapour–liquid nucleation properties for spherical and chain-like fluids by density functional theory*

Fu Dong(付 东)† and Liao Tao(廖 涛)

School of Environmental Science and Engineering, North China Electric Power University, Baoding 071003, *China*

(Received 23 March 2007; revised manuscript received 15 April 2007)

The excess Helmholtz free energy functional for nonpolar chain-like molecules is formulated in terms of a weighted density approximation (WDA) for short-range interactions and a Weaks–Chandler–Andersen (WCA) approximation and a Barker–Henderson (BH) theory for long-range attraction. Within the framework of density functional theory (DFT), vapour–liquid interfacial properties including density profile and surface tension, and vapour–liquid nucleation properties including density profile, work of formation and number of particles are investigated for spherical and chain-like molecules. The obtained vapour–liquid surface tension and the number of particles in critical nucleus for Lennard-Jones (LJ) fluids are consistent with the simulation results. The influences of supersaturation, temperature and chain length on vapour–liquid nucleation properties are discussed.

Keywords: vapour–liquid nucleation, chain like fluids, density functional theory
PACC: 6460Q, 7115J

1. Introduction

Nucleation is the first appearance of a new phase during a first-order transition and plays an important role in materials science, atmospheric sciences and biology.[1−4] Vapour–liquid nucleation is of fundamental as well as practical importance and great efforts have been devoted to understanding the vapour–liquid nucleation properties including density profiles across the nucleus, work of formation, number of particles and nucleation rate in recent years. Besides the experimental technology,[5−17] computer simulation techniques,[18−25] classical nucleation theory (CNT)[26−30] and density functional theory (DFT)[31,32] are routinely used to study these inhomogeneous properties.

Molecular dynamics (MD) and Monte Carlo (MC) simulation techniques have been used to simulate the critical supersaturation, density distribution from supersaturated gas to the centre of the liquid, the number of particles in critical nuclei and work of formation for Lennard-Jones (LJ)[18−23] and water.[24] Yasuoka *et al*[25] have simulated the nucleation properties for LJ fluids confined in slit pores using the MD method and showed that at a given supersaturation and temperature, nucleation rate for confined LJ fluid is greater than that for unconfined LJ fluid. While the simulation approaches are efficient to describe the vapour–liquid nucleation properties for spherical fluids, their usage is restricted to long chain molecules due to the computational intensive nature.

The classical nucleation theory has been extensively used to investigate the vapour–liquid nucleation properties in early studies.[26−30] In the CNT, the critical vapour–liquid nuclei are treated as droplets with dividing surface separating the new and old phases. Molecules within the dividing surface are treated as part of the bulk phase. Due to lack of the knowledge of microscopic cluster properties, the work required to get over the energy barrier and form the nucleus is calculated by using the experimental results of bulk properties and surface tension. It has two important limitations. One is that the energy barrier to nucleation at a spinodal must vanish, but this is not predicted by the CNT, the other is that even for an interface sharply curved in realistic situations, the CNT treats it as an infinite planar surface hence it is inaccurate for small critical nuclei. Although the CNT is easy to use, it predicts the nucleation rate too low at low temperatures and too high at high temperatures.

*Project supported by the National Natural Science Foundation of China (Grant Nos 20576030 and 20606009), the Program for New Century Excellent Talents of China (Grant No 06-0206), and the Research Fund of Key Laboratory for Nanomaterials, Ministry of Education of China (Grant No 2006-2).
†E-mail: fudong@tsinghua.org.cn

The DFT[31,32] is theoretically better than the CNT for vapour–liquid nucleation because it correctly predicts the critical energy that vanishes at the spinodal and it allows more realistic treatment of curvature effects and small clusters. A self-consistent DFT can be well reduced to bulk phase and applicable for interfacial properties, hence the bulk properties and surface tension required in the investigation of nucleation properties can be predicted and are no longer dependent on experiments. Moreover, compared with the simulation techniques, the DFT is able to quantitatively capture all the characteristics of the structure and inhomogeneous properties with the advantage of low computational cost. The basic framework for investigating the vapour–liquid nucleation properties using the DFT has been established by Oxtoby and coworkers in the early 1980s. From then on, the DFT has been extensively used in this field and become the basis of the theoretical understanding of vapour–liquid nucleation properties.[33−47]

In this work, an equation of state (EOS) applicable for both uniform and non-uniform fluids is constructed for chain-like fluids by using a weighted density approximation (WDA)[48−50] for short-range interactions and a Weaks–Chandler–Andersen (WCA) approximation and a Barker–Henderson (BH) theory[51] for long-range attraction. In the framework of DFT,[52−66] the vapour–liquid nucleation properties for LJ and chain-like fluids are investigated and the influences of supersaturation, temperature and chain length on the work of formation and number of particles for vapour–liquid nucleation are discussed.

The remainder of this paper is organized as follows. In Section 2, the density functional theory for chain-like molecules is introduced. In Section 3, numerical results for interfacial and nucleation properties are shown together with discussion. Finally, a short conclusion is given in the last section.

2. Theory

In the absence of an external potential, the grand potential $\Omega[\rho_M(\boldsymbol{R})]$ for chain-like fluids is expressed as

$$\Omega[\rho_M(\boldsymbol{R})] = F[\rho_M(\boldsymbol{R})] - \mu \int \rho_M(\boldsymbol{R}) \mathrm{d}\boldsymbol{R}, \quad (1)$$

where M represents the number of segments for each chain-like molecule; $\boldsymbol{R} \equiv (r_1, r_2, \cdots, r_M)$ denotes the position of M segments; r_i is the spatial position of the ith segment; $\rho_M(\boldsymbol{R})$ is the molecule density as a function of segment positions $\boldsymbol{R}$; μ is the chemical potential. The intrinsic Helmholtz free energy functional, $F[\rho_M(\boldsymbol{R})]$, is usually separated into two contributions: the ideal part and the excess part, i.e.

$$F[\rho_M(\boldsymbol{R})] = F^{\mathrm{id}}[\rho_M(\boldsymbol{R})] + F^{\mathrm{ex}}[\rho_M(\boldsymbol{R})]. \quad (2)$$

The ideal gas part of the Helmholtz free energy functional is exactly given as

$$\beta F^{\mathrm{id}} = \int \rho_M(\boldsymbol{R})[\ln \rho_M(\boldsymbol{R}) - 1 + V_{\mathrm{b}}(\boldsymbol{R})] \mathrm{d}\boldsymbol{R}, \quad (3)$$

where $\beta = 1/(kT)$, k is the Boltzmann constant and T is the absolute temperature. $V_{\mathrm{b}}(\boldsymbol{R}) \approx \sum_{i=1}^{M-1} v_{\mathrm{b}}(|r_{i+1} - r_i|)$ specifies the intramolecular interaction with the bonding potential v_{b} given by

$$\exp[-\beta v_{\mathrm{b}}(|r - r'|)] = \frac{\delta(|r - r'| - \sigma)}{4\pi\sigma^2}, \quad (4)$$

where σ is the diameter of segment in each chain-like molecule.

The excess Helmholtz free energy functional is formulated as

$$F^{\mathrm{ex}}[\rho_M(\boldsymbol{R})] = F^{\mathrm{hs}}[\rho_M(\boldsymbol{R})] + F^{\mathrm{chain}}[\rho_M(\boldsymbol{R})] + F^{\mathrm{att}}[\rho_M(\boldsymbol{R})], \quad (5)$$

where F^{hs}, F^{chain} and F^{att} represent the free energy functional for hard-sphere repulsion, chain connectivity and attractive interaction, respectively. Using the weighted density approximation, F^{hs} and F^{chain} are respectively as

$$F^{\mathrm{hs}}[\rho_M(\boldsymbol{R})] = \int \rho(r) f^{\mathrm{hs}}[\bar{\rho}(r)] \mathrm{d}r, \quad (6)$$

$$F^{\mathrm{chain}}[\rho_M(\boldsymbol{R})] = \int \rho(r) f^{\mathrm{chain}}[\bar{\rho}(r)] \mathrm{d}r, \quad (7)$$

where $f^{\mathrm{hs}}[\bar{\rho}(r)]$[67] and $f^{\mathrm{chain}}[\bar{\rho}(r)]$[68,69] are the excess Helmholtz free-energy density of hard-sphere and chain connectivity corresponding to a given density $\bar{\rho}(r) = \int \rho(r') w(|r - r'|) \mathrm{d}r'$ responsible for the excluded volume effect. For the correction of short-range interactions, the modified fundamental measure theory (MFMT) proposed by Yu and Wu[70,71] not only retains all the advantages of the original FMT but also improves structural and thermodynamic properties of hard-sphere fluids in the bulk under inhomogeneous conditions. Application of the MFMT to the thermodynamic properties of fluids confined in slit pores shows that the MFMT correctly captures all the oscillations of density profiles hence it can describe the phase behaviour more accurately.[72−75] However, for the investigation of vapour–liquid surface without an

external potential, the WDA provides an inerrant yet simple approach. In this work, the WDA is used for the correction of short-range interactions with the weight function given by

$$w(r) = \frac{3\Theta(\sigma - r)}{4\pi\sigma^3}. \tag{8}$$

The attractive contribution to the Helmholtz free energy functional is formulated as follows:

$$F^{\mathrm{att}}[\rho(r)] = -\frac{1}{2}\iint \mathrm{d}r'\mathrm{d}r u^{\mathrm{WCA}}(|r - r'|)\rho(r)\rho(r'), \tag{9}$$

where the WCA potential is expressed as

$$u^{\mathrm{WCA}}(|r - r'|) = \begin{cases} -\varepsilon, & |r - r'| \le r_{\min}, \\ 4\varepsilon\Big(\dfrac{\sigma^{12}}{|r - r'|^{12}} \dfrac{\sigma^6}{|r - r'|^6}\Big), & r_{\mathrm{c}} \ge |r - r'| > r_{\min}, \end{cases} \tag{10}$$

where r_{c} is the cut-off length and $r_{\min} = \sqrt[6]{2}\sigma$. As the WCA potential is used here, an effective hard-sphere diameter d instead of σ is used[51]

$$\frac{d}{\sigma} = \frac{0.3837 + 1.068/T^*}{0.4293 + 1/T^*}, \tag{11}$$

where $T^* = kT/\varepsilon$ is the reduced temperature and ε is the dispersion energy parameter.

At equilibrium, the grand potential is an extremum with respect to change in the density distribution

$$\frac{\delta\Omega[\rho_M(\boldsymbol{R})]}{\delta\rho_M(\boldsymbol{R})} = 0. \tag{12}$$

Therefore, the equilibrium density distribution is given by

$$\rho_M(\boldsymbol{R}) = \exp\Big\{\beta\Big(\mu - V_{\mathrm{b}}(\boldsymbol{R}) - \frac{\delta F^{\mathrm{ex}}[\rho_M(\boldsymbol{R})]}{\delta\rho_M(\boldsymbol{R})}\Big)\Big\}. \tag{13}$$

The chain segment density is defined as

$$\rho(r) = \int \sum_{i=1}^{M} \delta(r - r_i)\rho_M(\boldsymbol{R})\mathrm{d}\boldsymbol{R}. \tag{14}$$

By substituting expression (13) into expression (14), we have

$$\rho(r) = \exp(\beta\mu)\int \sum_{i=1}^{M} \delta(r - r_i) \times \exp\Big\{-\beta V_{\mathrm{b}}(\boldsymbol{R}) - \beta\frac{\delta F^{\mathrm{ex}}[\rho_M(\boldsymbol{R})]}{\delta\rho_M(\boldsymbol{R})}\Big\}\mathrm{d}\boldsymbol{R} \tag{15}$$

with

$$\frac{\delta F^{\mathrm{ex}}[\rho_M(\boldsymbol{R})]}{\delta\rho_M(\boldsymbol{R})} = \sum_{i=1}^{M}\int \frac{\delta F^{\mathrm{ex}}[\rho_M(\boldsymbol{R})]}{\delta\rho(r')}\delta(r' - r_i)\mathrm{d}r'. \tag{16}$$

By substituting Eqs.(4) and (16) into expression (15) and defining

$$\lambda(r_i) = \frac{\delta F^{\mathrm{ex}}[\rho_M(\boldsymbol{R})]}{\delta\rho(r')},$$

we have

$$\rho(r) = \exp(\beta\mu)\int \sum_{i=1}^{M} \delta(r - r_i) \times \exp[-\beta V_{\mathrm{b}}(\boldsymbol{R}) - \beta\sum_{j=1}^{M}\lambda(r_j)]\mathrm{d}\boldsymbol{R}. \tag{17}$$

3. Results and discussion

In the bulk phase, $F^{\mathrm{hs}}[\rho_M(\boldsymbol{R})]$ is reduced to the Carnahan–Starling equation,[67] $F^{\mathrm{id}}[\rho_M(\boldsymbol{R})]$, $F^{\mathrm{chain}}[\rho_M(\boldsymbol{R})]$ and $F^{\mathrm{att}}[\rho_M(\boldsymbol{R})]$ become

$$F^{\mathrm{id}}/NkT = \ln(\rho_M^{\mathrm{b}}\Lambda^3 - 1), \tag{18}$$

$$F^{\mathrm{chain}}/NkT = (1 - M)\ln[g^{\mathrm{hs}}(d)], \tag{19}$$

$$F^{\mathrm{att}}/NkT = \frac{\beta}{2}M^2\rho_M^{\mathrm{b}}\int 4\pi r^2 u^{\mathrm{WCA}}(r)\mathrm{d}r, \tag{20}$$

where $\beta = 1/(kT)$; $g^{\mathrm{hs}}(d) = (1 - 0.5\eta)/(1 - \eta)^2$ is the radial distribution function; $\eta = (\pi/6)M\rho_M^{\mathrm{b}}d^3$ is the packing factor; ρ_M^{b} is the molecule density in bulk phase.

Equations (18), (19) and (20) together with the Carnahan–Starling equation construct the EOS for uniform nonpolar chain-like fluids and the phase equilibria, chemical potential μ and the pressure p^{coex} for bulk phases at a given temperature can be determined. Using the chemical potential as an input, Eq.(17) is solved by using the Picard iteration method with a certain initial guess at density profile. Once the equilibrium density distribution is obtained, the grand potential in Eq.(1) can be rewritten as

$$\beta\Omega[\rho_M(\boldsymbol{R})] = \beta F^{\mathrm{ex}}[\rho_M(\boldsymbol{R})] - \int \mathrm{d}\boldsymbol{R}\rho_M(\boldsymbol{R}) - \int \mathrm{d}r\rho(r)\frac{\delta\beta F^{\mathrm{ex}}[\rho_M(\boldsymbol{R})]}{\delta\rho(r)}. \tag{21}$$

From Eq.(21), the excess grand potential can be determined and the interfacial and nucleation properties can be calculated subsequently.

3.1. Vapour–liquid surface tension

For a vapour–liquid surface, the initial guess at density profile is as follows:

$$\rho_M(z) = \begin{cases} \rho_M^{\mathrm{l}}, & z \le 0, \\ \rho_M^{\mathrm{v}}, & z > 0, \end{cases} \tag{22}$$

where ρ_M^{l} and ρ_M^{v} are the equilibrium molecule densities in liquid and vapour phases, respectively.

The surface tension is given by

$$\gamma = \frac{\Delta\Omega[\rho_M(z)]}{A} = \frac{\Omega[\rho_M(z)] + p^{\mathrm{coex}}V}{A}, \tag{23}$$

where $\rho_M(z)$ is the equilibrium molecule density across the vapour–liquid surface, A and V denote the surface area and volume, respectively.

Figure 1(a) shows the reduced vapour–liquid surface tension ($\gamma^* = \gamma\sigma^2\varepsilon$) and the corresponding density profile for LJ fluids. One may find from Fig.1(a) that the density profile varies smoothly between the bulk densities and the qualitative feature of the dependence of the surface tension on temperature is correctly captured. Because the short-range interaction is corrected by the WDA and the long-range attraction is expressed by BH theory with WCA potential, the surface tensions predicted by the present DFT are consistent with the simulation results. Figure 1(b) shows the vapour–liquid surface tension for chain-like fluids. From Fig.1(b), one finds that the surface tension for each chain-like fluid decreases with the increase of temperature. At a given temperature, the surface tension increases with the increase of chain length. In addition, the longer the chain length, the higher the temperature at which the vapour–liquid surface vanishes ($\gamma^* = 0$).

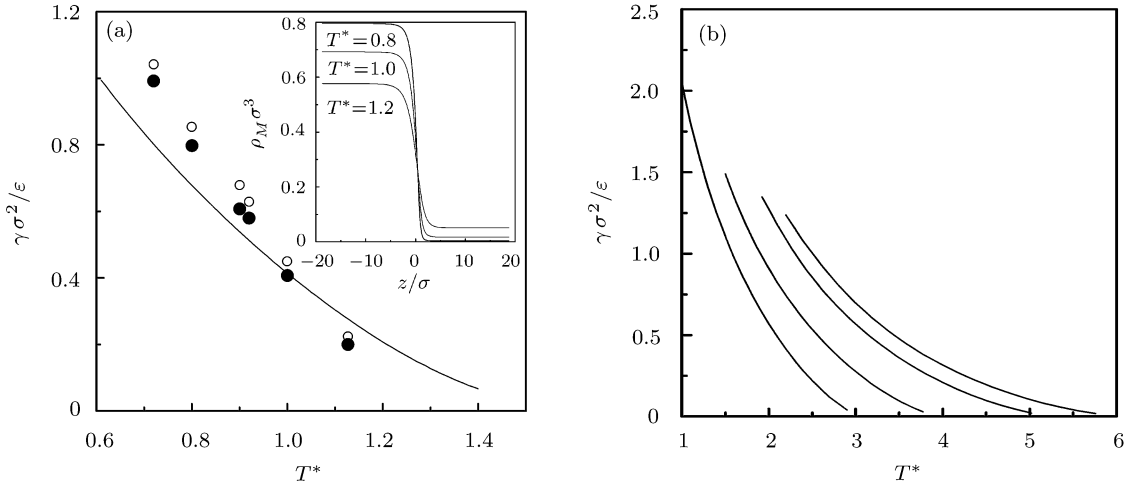


Fig.1. Fig.1 Interfacial properties for spherical and chain-like fluids in vapour–liquid surface. —: predicted by DFT. (a) surface tension and density profile (insert plot) for LJ fluids. ○, ●: simulation results;[76] (b) surface tensions for chain-like fluids with different chain lengths (from left to right, M = 3, 5, 10 and 15, respectively).

3.2. Vapour–liquid nucleation properties

When the vapour–liquid surface tensions are available, the initial guess at density profile for vapour–liquid nuclei can be expressed as follows:

$$\rho_M(r) = \begin{cases} \rho_M^{\mathrm{l}}, & 0 \le r \le r_0, \\ \rho_M^{\mathrm{sv}}, & r > r_0, \end{cases} \tag{24}$$

where $r_0 = 2\gamma/(kT\rho_M^{\mathrm{l}}\ln S)$ with $S = p/p^{\mathrm{coex}}$ being the supersaturation and ρ_M^{sv} being the molecule densities for the supersaturated gas surrounding the liquid droplets.

Once the equilibrium density profile from the supersaturated gas to the droplet centre is obtained, the work of formation and number of particles can be calculated from

$$\Delta\Omega[\rho_M(\boldsymbol{R})] = \Omega[\rho_M(\boldsymbol{R})] - \Omega[\rho_M^{\mathrm{sv}}], \tag{25}$$

$$n_{\mathrm{e}} = \int_0^\infty 4\pi r^2[\rho_M(r) - \rho_M^{\mathrm{sv}}]\mathrm{d}r. \tag{26}$$

The nucleation rate is then given by

$$J = J_0 \exp\Big[\frac{-\Delta\Omega[\rho_M(\boldsymbol{R})]}{kT}\Big]$$

with

$$J_0 = \sqrt{2\gamma/(\pi m)}\rho_M^{\mathrm{v}2}/\rho_M^{\mathrm{l}}, \tag{27}$$

where m is the molecular weight.

3.2.1. Nucleation properties for LJ fluids

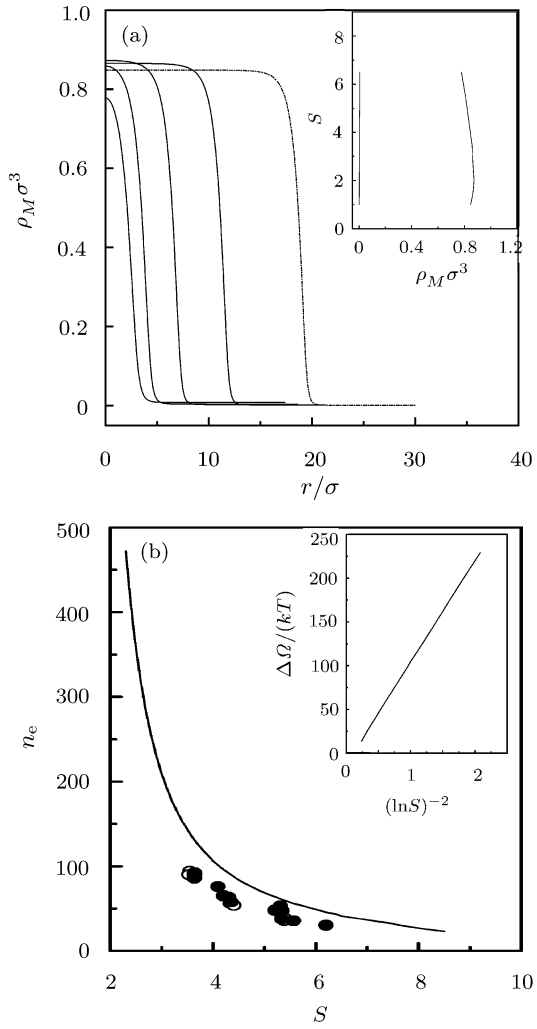


Fig.2. Vapour-liquid nucleation properties for LJ fluids at $T^* = 0.694$. (a) density profiles (from right to left, $S = 1.0$, 1.5, 2.0, 3.5 and 6.5, respectively) and the densities in the droplet centre and in supersaturated gas (insert plot); (b) number of particles and work of formation (insert plot), ○, ●: simulation results,[18] —: predicted by DFT.

Figures 2(a) and 2(b) show the vapour–liquid nucleation properties for LJ fluids at $T^* = 0.694$. Figure 2(a) presents the density profiles across the supersaturated gas and droplet centre under different supersaturations. In the case of saturation ($S = 1$), the density profile reduces to that for vapour–liquid surface as shown by the dashed line. With the decrease of S, the density profiles broaden, which indicates that the nuclei have a larger size in the case of lower pressures. The insert plot in Fig.2(a) shows the densities in the droplet centre ($r = 0$) and in supersaturated gas. In the case of saturation, the densities reduce to the coexistent vapour and liquid densities that can be determined according to the principle that the temperatures, chemical potentials and pressures in vapour and liquid phases should be equal. When the gas phase is supersaturated ($S > 1$), it is clearly demonstrated by the insert plot that the densities in the droplet centre first increase and then decrease with the increase of S, while those in the supersaturated gas increase monotonically with the increase of S. When the pressure is sufficiently high, the larger the S, the steeper the density profile with lower densities in the droplet centre and higher densities in the surrounding supersaturated gas. Figure 2(b) presents the predicted number of particles and work of formation. The insert plot indicates that the work of formation predicted by the DFT has linear relationship with $(\ln S)^{-2}$ and it decreases monotonically with the increase of S. From Fig.2(b), one also finds that although there is obvious deviation between the predicted number of particles and that from simulation results, the presented DFT correctly captures the qualitative feature that the number of particles is a function of supersaturation.

Figure 3 shows the number of particles, work of formation and densities in droplet centre and in supersaturated gas for LJ fluids at different temperatures. One finds that at a given supersaturation, $S = 2.5$, the number of particles and the work of formation decrease monotonically with the increase of temperature. The insert plot in Fig.3 shows that the density in droplet centre and that in supersaturated gas respectively decreases and increases monotonically with the increase of temperature.

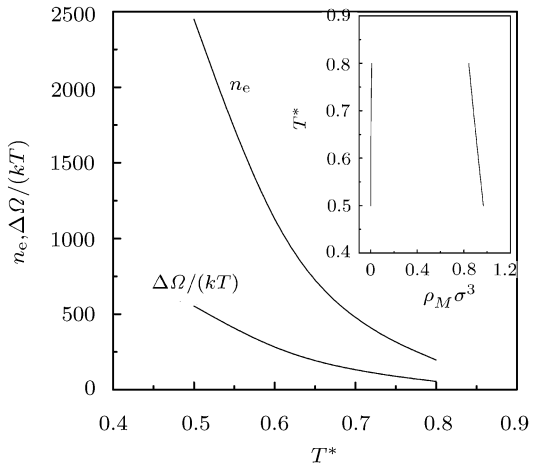


Fig.3. Number of particles, work of formation, and densities in the droplet centre and in supersaturated gas (insert plot) for LJ fluids at different temperatures. $S = 2.5$. —: predicted by DFT.

3.2.2. Nucleation properties for chain-like fluids

Figure 4 shows the number of particles and work of formation for short chain-like fluid with a chain length $M = 3$. We find that similar to spherical fluid, at a given temperature, the predicted number of particles for chain-like fluids decreases with the increase of S, and the predicted work of formation for chain-like fluids also has linear relationship with $(\ln S)^{-2}$ and it decreases monotonically with the increase of S. Also presented in this figure are, at a given supersaturation, the predicted number of particles and work of formation for chain-like fluids that tend to decrease with the increase of temperature. Moreover, with the increase of temperature, the supersaturation region in which the vapour–liquid nuclei stably exist becomes narrower. This indicates that at higher temperatures, the energy barrier to nucleation vanishes at lower values of S.

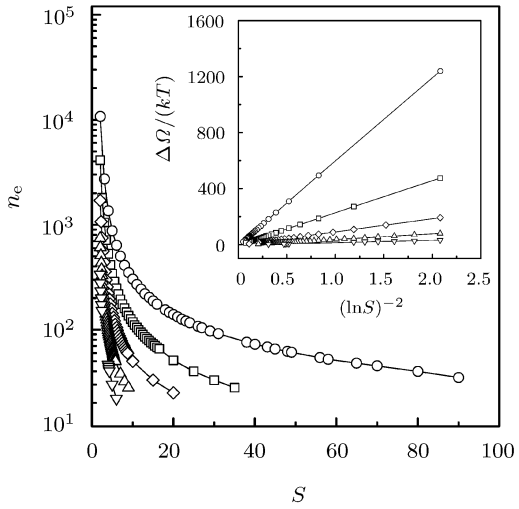


Fig.4. Number of particles and work of formation (insert plot) for chain-like fluids with $M = 3$. Symbols: predicted by DFT, ○: $T^* = 1.0$, □: $T^* = 1.2$, ◇: $T^* = 1.4$, △: $T^* = 1.6$ and ▽: $T^* = 1.8$. —: for guiding the eyes.

Figure 5(a) shows the relationship between temperature and the nucleation properties including the number of particles and work of formation for chain-like fluids with values of length M being 3, 5, 10 and 15. One finds from this figure that at a given supersaturation, both the number of particles and work of formation decrease with the increase of temperature. With the increase of chain length, the temperature at which the nuclei with a certain number of particles are formed turns higher. Figure 5(b) shows the relationship between the supersaturation and nucleation properties for chain-like fluids with values of chain length M being 5, 10 and 15. This figure indicates that at a given temperature, both the number of particles and work of formation decrease with the increase of supersaturation. Moreover, with the increase of chain length, the value of supersaturation under which the nuclei with a certain number of particles are formed becomes larger.

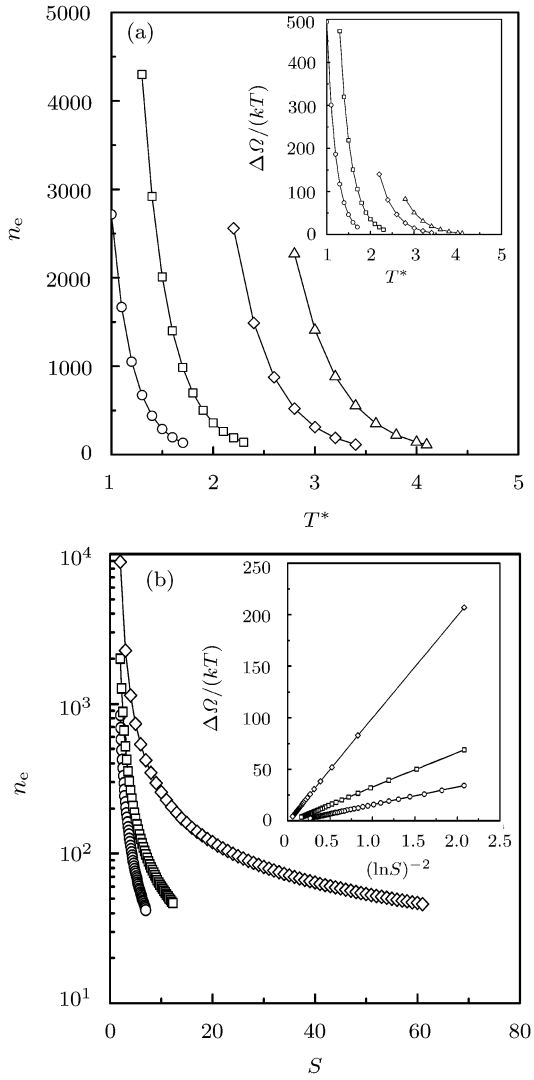


Fig.5. Number of particles and work of formation (insert plot) for different chain-like fluids. Symbols: predicted by DFT; —: for guiding the eyes. (a) $S = 3$ with the change of T^*, ○: $M = 3$, □: $M = 5$, ◇: $M = 10$, △: $M = 15$; (b) $T^* = 2.8$ with the change of S; ○: $M = 8$, □: $M = 10$, ◇: $M = 15$.

Figure 6 presents the influence of chain length on number of particles and work of formation. We find that at a given temperature and supersaturation, both the number of particles and work of formation

increase with the increase of chain length. A similar relationship can also be derived from CNT, in which the work of formation is formulated as $\Delta\Omega = 16\pi\gamma^3/(3(\rho^{\mathrm{l}}kT\ln S)^2)$ and the number of particles is formulated as $n_{\mathrm{e}}^{\mathrm{CNT}} = 32\pi\gamma^3/((3\rho^{\mathrm{l}})^2(kT\ln S)^3)$. At a given temperature, as the equilibrium surface tension γ and the equilibrium liquid density ρ^{l} respectively increases and decreases with the increases of chain length, both the number of particles and work of formation increase with the increase of chain length at a given supersaturation.

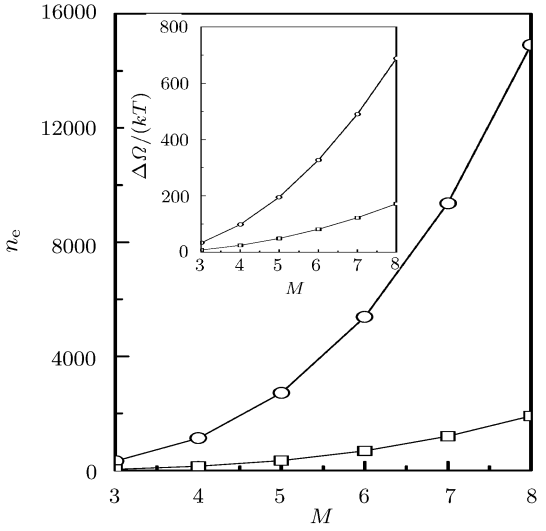


Fig.6. Number of particles and work of formation (insert plot) for different chain-like fluids at a given temperature and fixed supersaturations. Symbols: predicted by DFT, $T^* = 1.8$, ○: $S = 2$, □: $S = 4$; —: for guiding the eyes.

It is worth noting that during the calculation of the number of particles and the work of formation, the predicted vapour–liquid surface tensions only play a role in the initial guess at density profile. Moreover, the nuclear radius evaluated by $r_0 = 2\gamma/(kT\rho^{\mathrm{l}}_M \ln S)$ should be adjusted in calculation according to the methods well documented in the work of Oxtoby and Evans.[34] To calculate the nucleation rate from expression (27), the molecular parameters, for example, σ and ε for spherical molecules or σ and ε for each segment in chain-like molecules must be defined, so that the vapour–liquid surface tension γ can be determined.

4. Conclusion

In summary, an EOS is constructed by using WDA for short-range interaction and BH theory with WCA potential for long-range attraction. This EOS can be well reduced to bulk phase, and the surface tensions and density profiles for vapour–liquid surface and nucleation properties including the density profile, work of formation and number of particles can be investigated within the framework of DFT for chain-like fluids. A comparison of the predicted results with simulation results for LJ fluids shows that at low temperatures, the predicted surface tension and number of particles are respectively lower and higher than simulation results. This is due to the fact that our EOS is on the basis of mean field approximation. A more accurate EOS for vapour–liquid surface tension and nucleation properties may be constructed by combining the direct correlation function and the uniform EOS based on non-mean field approximation. As a comparison with simulation results shows that the current EOS correctly captures the qualitative features of the dependence of the surface tension on temperature and the dependence of number of particles on supersaturation, and the main purpose of the work is to qualitatively analyse the influences of supersaturation, temperature and chain length on vapour–liquid nucleation properties, we use this EOS for all the calculations in vapour–liquid nucleation properties. Our results show that the work of formation and the number of particles have similar behaviours. No matter whether or not the fluid is spherical or chain-like, these two properties decrease with the increase of temperature at a given supersaturation, and decrease with the increase of supersaturation at a given temperature. The chain length of molecules significantly affects the vapour–liquid surface tension and nucleation properties. The vapour–liquid surface tensions at a given temperature increase with the increase of chain length. At a given supersaturation and temperature, both the number of particles and work of formation increase with the increase of chain length.

References

[1] Boctttinger W J and Perepezko J H In: Das S K, Kear B H and Adam C M (ed) 1985 *Rapidly Solidified Crystalline Alloys* (Warrendale, PA: TMS-AIME) p263

[2] Wagner P E and Vali G 1988 *Atmospheric Aerosols and Nucleation* (Berlin: Springer)

[3] Toner M, Cravalho E G and Karel M 1990 *J. App. Phys.*

67 1582
[4] David W I F 1992 *J. Phys.: Con. Matt.* **4** 6087
[5] Zahoransky R A, Hoschele J and Steinwandel J 1999 *J. Chem. Phys.* **110** 8842
[6] Wegener P P, Clumpner J A and Wu J C 1972 *Phys. Flu.* **15** 1869
[7] Wu B J C, Wegener D D and Stein G D 1978 *J. Chem. Phys.* **68** 308
[8] Huang W, Zeng H Z, Zhang Y, Jiang S W, Wei X H and Li Y R 2005 *Acta Phys. Sin.* **54** 1334 (in Chinese)
[9] Wegener P P and Lee C F 1983 *J. Aero. Sci.* **14** 29
[10] Wagner P E and Strey R 1984 *J. Chem. Phys.* **80** 5266
[11] Adams G W, Schmitt J L and Zalabsky R A 1984 *J. Chem. Phys.* **81** 5074
[12] Adams G W, Chmitt J L S and Zalabsky R A 1983 *J. Chem. Phys.* **79** 4496
[13] Zang J C, Tian Z K, Liu Y H, Chi J, Zou Y L, Wei J Z and Ye J P 2006 *Acta Phys. Sin.* **55** 1358 (in Chinese)
[14] Wagner P E and Strey R 1982 *J. Aero. Sci.* **14** 381
[15] Strey R and Schmeling T 1986 *J. Chem. Phys.* **85** 6192
[16] Strey R, Wagner P E and Schmeling T 1986 *J. Chem. Phys.* **84** 2325
[17] Wo1lk J and Strey R 2001 *J. Phys. Chem.* B **105** 11683
[18] Laasonen K, Wonczak S, Strey R and Laaksonen A 2000 *J. Chem. Phys.* **113** 9741
[19] Zhukhovitskii D I 1995 *J. Chem. Phys.* **103** 9401
[20] Ten Wolde P R and Frenkel D 1998 *J. Chem. Phys.* **109** 9901
[21] Toxvaerd S 2001 *J. Chem. Phys.* **115** 8913
[22] Trokhymchuk A and Alejandre J 1999 *J. Chem. Phys.* **111** 8510
[23] Yasuoka K and Matsumoto M 1998 *J. Chem. Phys.* **109** 8451
[24] Yasuoka K and Matsumoto M 1998 *J. Chem. Phys.* **109** 8463
[25] Yasuoka K, Gao G T and Zeng C 2000 *J. Chem. Phys.* **112** 4279
[26] Frenkel J 1955 *Kinetic Theory of Liquids* (New York: Dover)
[27] Abraham F F 1974 *Homogeneous Nucleation Theory* (New York: Academic)
[28] Drossinos Y and Kevrekidis P G 2003 *Phys. Rev.* E **67** 26127
[29] Kashchiev D 2000 *Nucleation: Basic Theory with Applications* (Oxford: Butterworth-Heinemann)
[30] Debenedetti P G 1996 *Metastable Liquids: Concepts and Principles* (Princeton NJ: Princeton University Press)
[31] Evans R In: Henderson D (ed) 1992 *Fundamentals of Inhomogeneous Fluids* (Dekker: New York)
[32] Oxtoby D 2002 *Annu. Rev. Mater. Res.* **32** 39
[33] Harrowell P and Oxtoby D W 1984 *J. Chem. Phys.* **80** 1639
[34] Oxtoby D W and Evans R 1988 *J. Chem. Phys.* **89** 7521
[35] Zeng X C and Oxtoby D W 1991 *J. Chem. Phys.* **94** 4472
[36] Oxtoby D W and Harrowell P R 1992 *J. Chem. Phys.* **96** 3834
[37] Oxtoby D W and Kashchiev D 1994 *J. Chem. Phys.* **100** 7665
[38] Bagdassarian C K and Oxtoby D W 1994 *J. Chem. Phys.* **100** 2139
[39] Laaksonen A and Oxtoby D W 1995 *J. Chem. Phys.* **102** 5803
[40] Talanquer V and Oxtoby D W 1995 *J. Chem. Phys.* **102** 2156
[41] Nyquist R M, Talanquer V and Oxtoby D W 1995 *J. Chem. Phys.* **103** 1175
[42] Shen Y C and Oxtoby D W 1996 *J. Chem. Phys.* **105** 6517
[43] Shen Y C and Oxtoby D W 1996 *Phys. Rev. Lett.* **77** 3585
[44] Talanquer V and Oxtoby D W 1998 *J. Chem. Phys.* **109** 223
[45] Talanquer V, Cunningham C and Oxtoby D W 2001 *J. Chem. Phys.* **114** 6759
[46] Christopher P S and Oxtoby D W 2003 *J. Chem. Phys.* **119** 10330
[47] Napari I, Laaksonen A, Talanquer V and Oxtoby D W 1999 *J. Chem. Phys.* **110** 5906
[48] Tarazona P 1985 *Phys. Rev.* A **31** 2672
[49] Curtin W A and Ashcroft N W 1985 *Phys. Rev.* A **32** 2909
[50] Zhou S Q and Zhang X Q 2002 *Chin. Phys.* **11** 1051
[51] Verlet L and Weis J 1972 *J. Phys. Rev.* A **5** 939
[52] Chandler D, McCoy J D and Singer S J 1986 *J. Chem. Phys.* **85** 5971
[53] Donley J P, Curro J G and McCoy J D 1994 *J. Chem. Phys.* **101** 3205
[54] Sen S, Cohen J M, McCoy J D and Curro J G 1994 *J. Chem. Phys.* **101** 9010
[55] Donley J P, Rajasekaran J J, McCoy J D and Curro J G 1995 *J. Chem. Phys.* **103** 5061
[56] McCoy J D, Teixeira M A and Curro J G 2001 *J. Chem. Phys.* **114** 4289
[57] McCoy J D, Nath S K, Curro J G and Saunders R S 1998 *J. Chem. Phys.* **108** 3023
[58] Woodward C E 1991 *J. Chem. Phys.* **94** 3183
[59] Zhou S Q 2007 *Chin. Phys.* **16** 1167
[60] Yu Y X and Wu J Z 2002 *J. Chem. Phys.* **117** 2368
[61] Yu Y X and Wu J Z 2003 *J. Chem. Phys.* **118** 3835
[62] Li Z D, Cao D P and Wu J Z 2005 *J. Chem. Phys.* **122** 224701
[63] Cao D P and Wu J Z 2004 *J. Chem. Phys.* **121** 4210
[64] Cao D P, Jiang T and Wu J Z 2006 *J. Chem. Phys.* **124** 164904
[65] Ye Z C, Cai J, Liu H L and Hu Y 2005 *J. Chem. Phys.* **123** 194902
[66] Ye Z C, Chen H Y, Cai J, Liu H L and Hu Y 2006 *J. Chem. Phys.* **125** 124705
[67] Carnahan N F and Starling K E 1969 *J. Chem. Phys.* **51** 635
[68] Chapman W G, Gubbins K E, Jackson G and Radosz M 1989 *Fluid Phase Equilib.* **52** 31
[69] Huang S H and Radosz M 1990 *Ind. Eng. Chem. Res.* **29** 2284
[70] Yu Y X and Wu J Z 2002 *J. Chem. Phys.* **117** 10156
[71] Yu Y X, Wu J Z, Xin Y X and Gao G H 2004 *J. Chem. Phys.* **121** 1535
[72] Yu Y X, Wu J Z, You F Q and Gao G H 2005 *Chin. Phys. Lett.* **22** 246
[73] Yu Y X, Gao G H and Wang X L 2006 *J. Phys. Chem.* B **110** 14418
[74] Fu D 2006 *J. Chem. Phys.* **124** 164701
[75] Fu D and Li X S 2006 *J. Chem. Phys.* **125** 084716
[76] Trokhymchuk A and Alejandre J 1999 *J. Chem. Phys.* **111** 8510